

# Magnetic and Momentum Bias Attitude Control Design for the HETE Small Satellite

Daniel H. Chang\*  
*Massachusetts Institute of Technology  
Cambridge, MA.*

A design study of the attitude control system for the High Energy Transient Experiment (HETE) small satellite is presented. The satellite is 3-axis stabilized and sun pointing, with stringent pointing stability requirements. For actuation, magnetic torquers and a momentum wheel are chosen for their technological maturity and lack of consumables. One science instrument (CCD UV camera) and sun sensors provide attitude measurement. Two complimentary control strategies are implemented to maximize controllability given the expected wide variation in Earth field direction. As this actuator complement is particularly suitable for a variety of small satellite missions, the design guidelines presented here should be of use to many designers.

## I. Introduction

The combination of a momentum wheel and magnetic torquers for the attitude control subsystem's actuator complement is especially attractive for many small LEO satellites with moderately tight pointing and stability requirements. The loss of controllability about one axis when using magnetic torquers is offset by the wheel's torque control and gyroscopic stiffness. Desaturation of the wheel is accomplished without expendables, and the gyroscopic stiffness increases the range of Earth field vector directions for which the disturbance torque component associated with desaturating can be tolerated. Active nutation damping eliminates the need for a passive damper, saving mass. Most importantly, the hardware technology is mature and available in sizes suitable for small satellite needs.

The major issue which arises in the design of control laws for this actuator complement is the inherent time-varying controllability associated with the changing field vector. The directional variations are generally more pronounced for inertially stabilized satellites than for earth-pointing ones. Two complementary control strategies are studied in this paper to maximize controllability: "full authority" by algebraically summing magnetic and wheel torques, and "partial authority" using the traditional wheel + spin-axis coil combination. The advantage of using either depends on the encountered field direction, and quantitative penalty factors are derived for both. For orbit/attitude combinations where the field

vector changes sufficiently to warrant using both actuator modes, a criterion for switching between them is studied. For the partial authority mode, a control law based on gain-scheduling LQR solutions to the projection of the measure field vector on the wheel plane is found to be effective and quite easy to implement. The controllers shown here take advantage of currently available on-board processing capability to simplify design analysis and extend performance as compared to some earlier designs<sup>1,2,3</sup>.

This work is based on a design study of the on-orbit attitude control system for the High Energy Transient Experiment (HETE) small satellite. The mission goal is to provide a comprehensive study of high energy, short duration  $\gamma$ -ray, X-ray, and UV burst phenomena using a small, LEO satellite. The desired mission attitude is 3-axis inertially stabilized and sun-pointing. Since the mission orbit is of low inclination, science observations are made during orbit night while household maintenance such as battery charging and momentum management are performed during orbit day. Pointing requirements are loose ( $\sim 5^\circ$  for solar panels during orbit day; instruments are wide FOV), but the desired pointing stability for observations is tight (target is  $< 2^\circ/\text{hr}$ ). Attitude determination during orbit night shares star-identification functions included in the data reduction algorithms for the UV CCD instrument. During orbit day, an analog sun-sensor provides 2 axes of attitude information, which is sufficient. A 3-axis magnetometer measures the local field vector. Three  $4 \text{ Am}^2$  hollow-core torque coils and a y-axis momentum wheel form the actuator complement for the spacecraft.

HETE is a NASA Goddard sponsored project managed by the MIT Center for Space Research<sup>4</sup>, with contributing instrument/science teams from

---

\* Graduate Research Assistant, Dept. of Aeronautics/Astronautics. Currently Member of Technical Staff, Jet Propulsion Laboratory, Pasadena, CA. Member AIAA.

CNES, ISAS, Los Alamos, UC Berkeley, UC Santa Cruz, and U. of Chicago. Most of the preliminary spacecraft system design is credited to Aero/Astro Inc. of Herndon, VA., who are the spacecraft bus contractor. Launch on a Pegasus vehicle is currently scheduled for October 1994.

## II. Earth Field Geometry

The direction of the field vector in the spacecraft body frame is of key importance. Accordingly, the angles  $\Theta$  and  $\Psi$  are defined in Figure 1 below with respect to frame B, HETE's body-fixed frame. Note also that the momentum wheel axis is along  $B_2$ , and that the  $B_3$  is intended to point to the sun. The terms "axial" and "transverse" shall be used in the text to refer to directions along  $B_2$  and normal to  $B_2$  respectively.  $[\beta_1 \beta_2 \beta_3]$ , the components of the field vector  $\beta$ , are defined with respect to frame B unless otherwise noted.

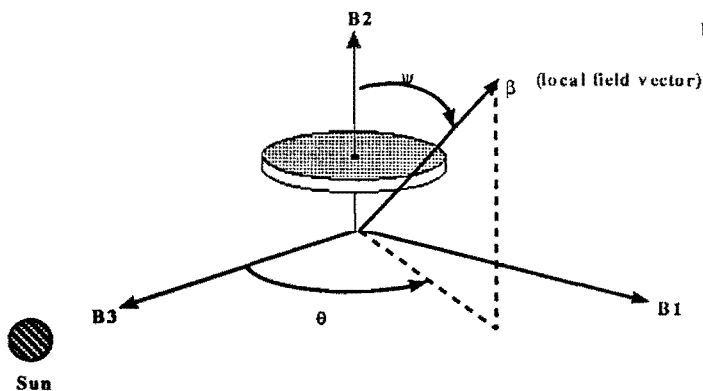


Figure 1: definition of  $\Theta$  and  $\Psi$  in frame B

Spacecraft designers typically refer to the Local Vertical - Local Horizontal (LVLH) frame for orbit-relative vector quantities, while the geologists use the North-East-Down (NED) frame when discussing the Earth's field. The two are related by a trivial transformation. We designate the LVLH frame as frame L and the NED frame as frame N.  $L_1$  is the local horizontal, which is also the velocity vector for circular orbits;  $L_3$  is the nadir, and  $L_2$  is the orbit normal and completes the dextral triad. Therefore, for a satellite in a prograde orbit,  $L_1 = N_2$ ,  $L_2 = -N_1$ , and  $L_3 = N_3$ . Two angles, the "declination" and the "dip," are frequently used to specify the field vector direction; they are defined in Figure 2.

Figures 3 A-C show, respectively, the total intensity, dip, and declination of the Earth field, from Ref. [8]. Although taken from surface data, the

plots are reasonably representative of the field at LEO. The planned HETE orbit is 555 Km at  $28^\circ$  inclination. It is seen from the figures that the total field intensity encountered for a  $28^\circ$  inclination orbit range approximately from  $20 \mu T$  to  $50 \mu T$ , with average around  $30 \mu T$ . The dip angle varies tremendously, at least  $\pm 50^\circ$ , and fairly uniformly about the magnetic equator, which is within  $\pm 10^\circ$  latitude of the equator except going by the SAA (South American Anomaly). The declination, however, is small- at worst  $20^\circ$ , but average somewhere between 0 and  $10^\circ$ . This suggests that, with respect to the NED frame, the North component is fairly constant and biased, the East component is small and unbiased, while the Down component will undergo large fluctuations with peaks greater than the North component.

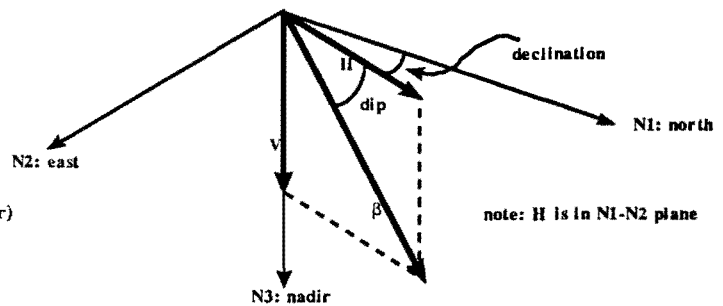


Figure 2: definition of declination and dip angles

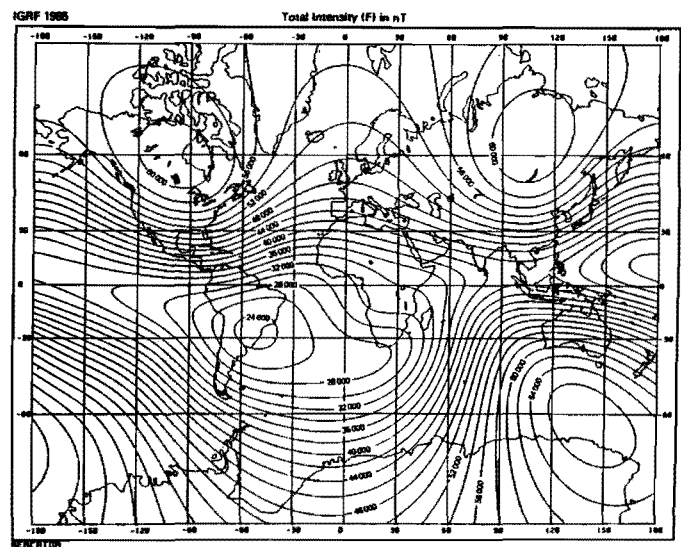


Figure 3A: surface field intensity (nT), from Ref. [8]

The field history WRT the body frame depends on the s/c attitude. For Earth-pointing missions, there may exist orbits where  $\Theta$  and  $\Psi$  remain fairly

constant, allowing for control strategies to be designed accordingly. However, for inertially fixed

### III. Actuator Strategies

As configured, the spacecraft can generate control torques according to (vectors expressed WRT frame **B**):

$$\begin{bmatrix} \tau_{c1} \\ \tau_{c2} \\ \tau_{c3} \end{bmatrix} = \begin{bmatrix} -m_3\beta_2 \\ m_3\beta_1 - m_1\beta_3 \\ m_1\beta_2 \end{bmatrix} + m_2 \begin{bmatrix} \beta_3 \\ 0 \\ -\beta_1 \end{bmatrix} + \begin{bmatrix} 0 \\ \tau_w \\ 0 \end{bmatrix} \quad [1]$$

Where  $\tau_w$  is the torque generated about the wheel axis,  $\underline{m}$  is the commanded dipole vector from the coils, and  $\underline{\beta}$  is the local Earth field. The constraint imposed by the cross product ( $\underline{m} \times \underline{\beta}$ ) is that the torque generated by the coils must lie in the plane orthogonal to the  $\underline{\beta}$  vector (it must also be perpendicular to  $\underline{m}$ , but this isn't really a constraint since  $\underline{m}$  can be chosen). The axial coil ( $m_2$ ) terms and transverse coils' terms are separated to suggest two actuator strategies:

"Full Authority Actuator Mode."

Here the wheel torque  $\tau_w$  is used in concert with the magnetic torque  $\tau_w$  to produce a sum torque vector which can point in arbitrary directions. Eq. [1] is augmented with the condition  $\underline{\beta} \cdot \underline{m} = 0$ ; this can be inverted to solve for  $\underline{m}$  and  $\tau_w$  given measured  $\underline{\beta}$  and commanded  $\underline{\tau}_c$ :

$$\begin{bmatrix} 0 & \beta_3 & -\beta_2 & 0 \\ -\beta_3 & 0 & \beta_1 & 1 \\ \beta_2 & -\beta_1 & 0 & 0 \\ \beta_1 & \beta_2 & \beta_3 & 0 \end{bmatrix} \begin{bmatrix} m_1 \\ m_2 \\ m_3 \\ \tau_w \end{bmatrix} = \begin{bmatrix} \tau_{c1} \\ \tau_{c2} \\ \tau_{c3} \\ 0 \end{bmatrix} \quad [2]$$

The  $\underline{\beta} \cdot \underline{m} = 0$  constraint forces  $\underline{m} \perp \underline{\beta}$ , as there is never a reason to impose a coil current penalty by choosing anything else. This makes the solution for  $\underline{m}$  unique. When  $\beta_2 \neq 0$ , the vector sum of  $\underline{m} \times \underline{\beta}$  and  $\underline{\tau}_w$  spans 3-space. Clearly, this actuator mode is inefficient when  $\Psi$  comes close to  $90^\circ$ , as large  $\tau_w$  and  $\underline{m}$  are then necessary to vectorally sum to a small  $\underline{\tau}_c$ . To quantify this, consider the solution for  $\tau_w$  from inverting eq. [2]:

$$\tau_w = \frac{1}{\beta_2} \begin{bmatrix} \beta_1 & \beta_2 & \beta_3 \end{bmatrix} \begin{bmatrix} \tau_{c1} \\ \tau_{c2} \\ \tau_{c3} \end{bmatrix} = \frac{1}{\cos(\Psi)} (\cos(\alpha) \|\underline{\tau}_c\|) \quad [3]$$

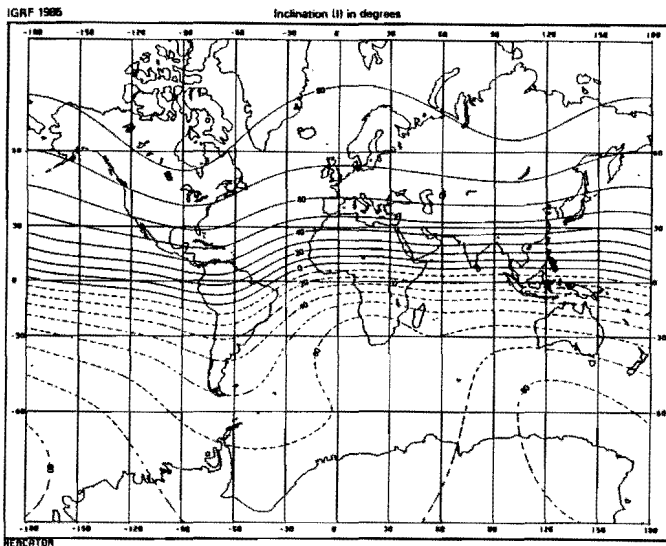


Figure 3B: surface field dip angle (in degrees; also referred to as inclination), from Ref. [8]

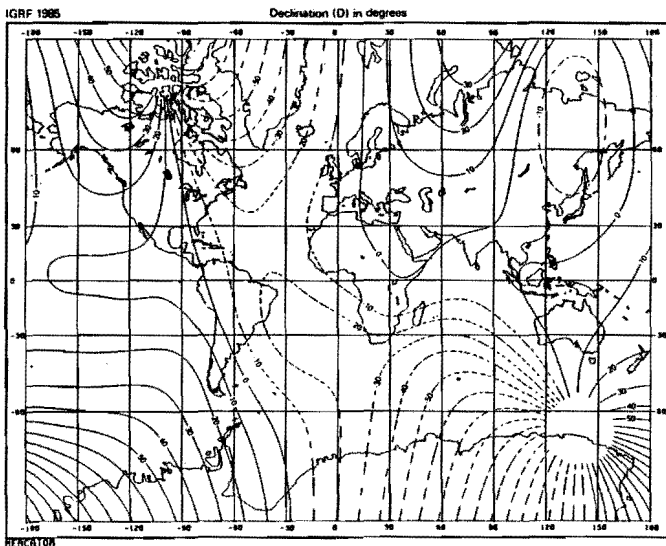


Figure 3C: surface field declination ( $^\circ$ ), from Ref. [8]

attitudes, node regression typically causes  $\Theta$  and  $\Psi$  to sweep most of their respective ranges by distributing the North and Down components of the field. This was found in simulations to be the case for HETE's orbit/attitude combination, even allowing for the degree of freedom from roll about the sun-vector. Therefore, controllers which will cope with large variations of the field direction must be designed.

where  $\alpha$  is the included angle between  $\beta$  and  $\tau_c$ , and  $\Psi$  is as defined in Figure 1. We see that the "penalty factor" of the full authority mode scales with the secant of  $\Psi$ .

*"Partial Authority Actuator Mode"*

Here the axial coil  $m_2$  is used to produce transverse torques,  $\tau_w$  produces axial torques, and the transverse coils are used for momentum management. Note this is the "traditional" magnetic control strategy.<sup>6</sup> The penalty is the additional constraint on the direction of achievable control torques. From [1], it is seen that  $m_2$  produces torques on the spin plane along  $\Theta \pm 90^\circ$ . Thus disturbance torques parallel to the spin plane projection of  $\beta$  cannot be canceled. The transverse coils generate wheel desaturation torques, along with an undesirable disturbance component in the spin plane proportional in magnitude to  $\beta_2$ . This is discussed below.

This actuator mode is inefficient when  $\Psi$  approaches 0, when the spin plane projection of  $\beta$  becomes too small for  $m_2$  to use. To quantify this, we solve for the required axial dipole  $m_2$  given the commanded transverse plane torque  $[\tau_1 \ 0 \ \tau_3]$ :

$$m_2 = \frac{\begin{vmatrix} \tau_{c1} & 0 & \tau_{c3} \\ \beta_3 & 0 & -\beta_1 \end{vmatrix}}{\begin{vmatrix} \tau_{c1} & 0 & \tau_{c3} \\ \beta_1 & \beta_2 & \beta_3 \end{vmatrix}} = \frac{1}{\sin(\Psi)} \left( \frac{\begin{vmatrix} \tau_{c1} & 0 & \tau_{c3} \\ \beta_1 & \beta_2 & \beta_3 \end{vmatrix}}{\begin{vmatrix} \tau_{c1} & 0 & \tau_{c3} \\ \beta_1 & \beta_2 & \beta_3 \end{vmatrix}} \right) \quad [4]$$

and it is seen that the "penalty factor" associated with the partial authority mode scales with the cosecant of  $\Psi$ .

*Actuator Mode Switching:*

In this design study, a combination of both actuator modes is used for orbit night, while only the partial authority mode is used for orbit day. Reasons for the latter include:

- The pointing requirement for orbit day is loose, and rate requirements are less stringent; therefore, turning off the  $m_2$  control loop for the brief periods (~100-500 sec from simulations using a high order field model) of bad field is an acceptable strategy.
- Wheel desaturation is easier in the partial authority mode.

To switch between actuator modes during orbit night, a wide Schmidt trigger (Figure 5) applied to  $\Psi$  is found to work well. The dependence of the penalty factors on the secant and cosecant of  $\Psi$

implies that a strong need to switch actuation modes only exists near the extremes of the  $\Psi$  range, as shown in Figure 4. This is fortunate because even though the full authority mode yields better disturbance rejection performance, control-law switching always excites undesirable transients. The philosophy, then, is to stay in the current mode as long as possible, until forced to switch by the field vector direction. The hysteresis also has usual the advantage of preventing control mode "flutter" when  $\Psi$  is on the verge of a transition point. Good trigger points are found in simulation to be about when the penalty reaches a factor of 3, which from Figure 4 correspond to  $\Psi$  values of  $20^\circ/160^\circ$  and  $70^\circ/110^\circ$ .

In summary, the dual actuator mode strategy outlined compensates for local field direction changes by in effect emphasizing the transverse coils to generate magnetic torque when  $\Psi$  is near 0 and the axial coil when  $\Psi$  is near  $90^\circ$ . The additional benefit of summing the wheel and mag torques when  $\Psi$  is near 0 is a bonus which is easily taken advantage of.

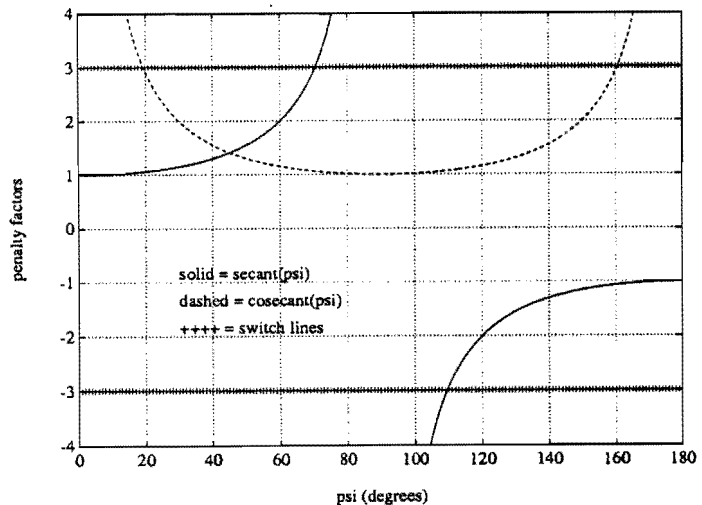


Figure 4- penalty factors for either actuator mode and switch lines used in simulations

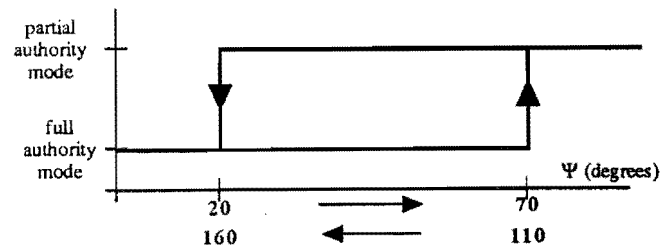


Figure 5- orbit night actuator mode switch law

## Wheel Momentum Management

Desaturation<sup>1</sup> of the wheel requires generation of magnetic torques about the spin axis, which is usually accompanied by an undesirable disturbance torques component. It is seen that the transverse coil mag. moments  $m_1$  and  $m_3$  generate torques according to:

$$\underline{\tau} = \begin{bmatrix} 0 \\ m_3\beta_1 - m_1\beta_3 \\ 0 \end{bmatrix} + \beta_2 \begin{bmatrix} -m_3 \\ 0 \\ m_1 \end{bmatrix} \equiv \underline{\tau}_{ds} + \underline{\tau}_d \quad [5]$$

where  $\underline{\tau}_{ds}$  is the desired desaturation torque, and  $\underline{\tau}_d$  is the associated disturbance on the spin plane. The optimal coil commands for desaturation given a measured field vector  $\beta$  can therefore be formulated simply as a linear Lagrange multiplier problem:

Minimize:

$$\left\| \beta_2 \begin{bmatrix} -m_3 \\ 0 \\ m_1 \end{bmatrix} + m_2 \begin{bmatrix} \beta_3 \\ 0 \\ -\beta_1 \end{bmatrix} \right\|^2 \quad [6]$$

subject to the constraint:

$$\begin{bmatrix} -\beta_3 & \beta_1 \end{bmatrix} \begin{bmatrix} m_1 \\ m_3 \end{bmatrix} = \tau_{ds} \quad [7]$$

where the scalar  $\tau_{ds}$  here denotes the desired desaturation torque as requested by the controller. The torque due to the axial coil moment  $m_2$  is included in the cost function [6] to investigate the possibility of using the axial coil to offset the disturbance component due to the transverse coils. Imbedding the cost function to the constraint give the following solution for the coil moments:

$$\begin{bmatrix} m_1 \\ m_3 \end{bmatrix} = \left( \frac{\tau_{ds}}{\beta_1^2 + \beta_3^2} \right) \begin{bmatrix} -\beta_3 \\ \beta_1 \end{bmatrix} \quad [8a]$$

$$m_2 = 0 \quad [8b]$$

<sup>1</sup>In HETE's case the term "desaturation" is used misleadingly, since the mission plan is to bring the wheel momentum close to nominal every orbit day, optimizing controller performance during orbit night when science observations occur. At no time will enough momentum be permitted to accumulate on the wheel to "saturate" it.

That the solution for the axial coil is zero implies that it cannot be used to lessen the magnitude of the disturbance torque associated with desaturation. Substitution of [8a] into [5] gives:

$$\underline{\tau}_d = -\beta_2 \begin{pmatrix} \frac{\tau_{ds}}{\beta_1^2 + \beta_3^2} \\ 0 \\ \beta_3 \end{pmatrix} \quad [9]$$

which shows that  $\underline{\tau}_d$  points along the projection of the field vector onto the spin plane. These relations are summarized in Figure 6.

The efficiency of desaturation is again a function of  $\Psi$ . The desaturation "efficiency" can be expressed as the ratio of disturbance to desaturation torque  $\frac{\|\underline{\tau}_d\|}{\|\underline{\tau}_{ds}\|}$ , with zero therefore being the optimum value. Recall from [5]:

$$\|\underline{\tau}_d\| = \beta_2 \sqrt{m_1^2 + m_3^2} \quad [10]$$

Recall also, by definition,  $|\underline{\tau}_{ds}| = \tau_{ds}$ . Equation [7] expresses the scalar  $\tau_{ds}$  in the form of a vector dot product. But since [8a] states that  $m_1$  and  $m_3$  are to be chosen such that:

$$\begin{bmatrix} -\beta_3 \\ \beta_1 \end{bmatrix} \cdot \begin{bmatrix} m_1 \\ m_3 \end{bmatrix} \quad [11]$$

the cosine of the included angle of this dot product is 1, and consideration of Figure 1 then produces the desired form:

$$\frac{\|\underline{\tau}_d\|}{\|\underline{\tau}_{ds}\|} = \frac{\beta_2}{\sqrt{\beta_1^2 + \beta_3^2}} = \frac{1}{\tan(\Psi)} \quad [12]$$

Thus the efficiency of the desaturation coil commands scale with the co-tangent of  $\Psi$ , with  $\Psi = 90^\circ$  being optimal. As seen in Figure 7, there is again a fortunately wide range of  $\Psi$  when the penalty is acceptable.

The desaturation control law is chosen to be as simple as possible. The dynamics between  $\underline{\tau}_{ds}$  and  $\delta\Omega$  is  $1/I_{ws}$ , which cannot be driven closed loop unstable for any loop gain of the correct sign. The desaturation control algorithm, implemented during orbit day in parallel with the attitude control loop which uses the partial authority actuator mode, is simply:

•  $\tau_{ds} = -K(\delta\Omega)$ ,  $K > 0$ .  $K$  is chosen such that the time constant  $I_w/K = 1000$  sec. in this design. Coil commands  $m_1$  and  $m_3$  are then computed using eq. [8a].

•  $\Psi$  is monitored on line to limit  $K$  so as to not violate a threshold on  $|\tau_d|$  as calculated by Eq. [12]. For this design,  $|\tau_d|_{\max} = 40 \mu\text{Nm}$  is found to work well in simulation.

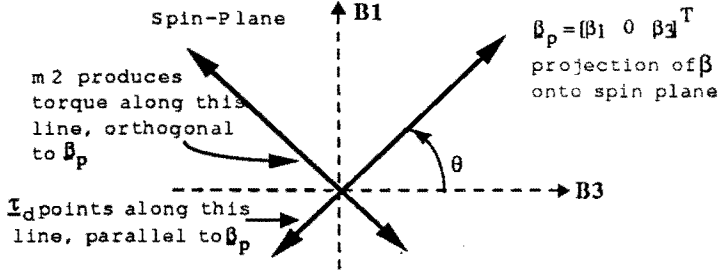


Figure 6: coil torques produced on the spin-plane

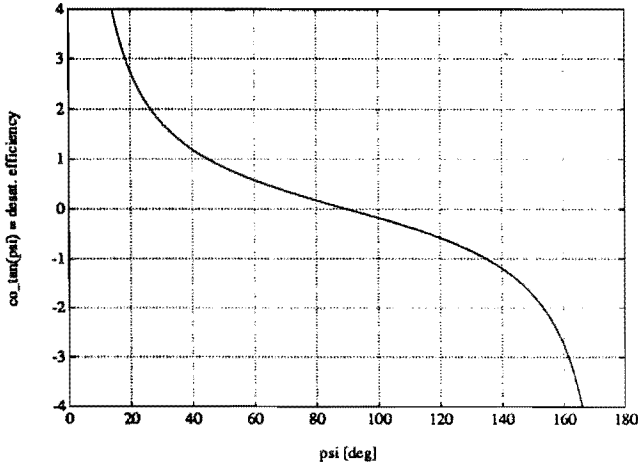


Figure 7: efficiency of transverse coils at generating desaturation torques as function of  $\Psi$

#### IV. Dynamics Issues

For completeness sake, the equations of motion and design plant model (DPM) for control design are given below. A rigid body assumption is entirely adequate for HETE. Define the following:

$I_1, I_2, I_3$  = principal moments of inertia for s/c + wheel system

$I_w$  = axial wheel moment of inertia

$\Omega_0$  = nominal wheel spin rate

$\delta\Omega$  = deviation from  $\Omega_0$

$h_w = I_w(\Omega_0 + \delta\Omega)$

$C_{PB}$  = transformation matrix from body frame  $B$  to principal frame  $P$

$H$  = system angular momentum in frame  $P$

$$C_{PB} = \begin{bmatrix} c_{11} & c_{12} & c_{13} \\ c_{21} & c_{22} & c_{23} \\ c_{31} & c_{32} & c_{33} \end{bmatrix} \quad [13a]$$

$$H = \begin{bmatrix} I_1\omega_1 \\ I_2\omega_2 \\ I_3\omega_3 \end{bmatrix} + C_{PB} \begin{bmatrix} 0 \\ I_w(\Omega_0 + \delta\Omega) \\ 0 \end{bmatrix} \quad [13b]$$

$$\begin{bmatrix} \tau_1 \\ \tau_2 \\ \tau_3 \end{bmatrix} = C_{PB} \left\{ \begin{bmatrix} -m_3\beta_2 \\ m_3\beta_1 - m_1\beta_3 \\ m_1\beta_2 \end{bmatrix} + m_2 \begin{bmatrix} \beta_3 \\ 0 \\ -\beta_1 \end{bmatrix} + \begin{bmatrix} 0 \\ I_w \frac{d\delta\Omega}{dt} \\ 0 \end{bmatrix} \right\} \quad [13c]$$

$$\frac{dH}{dt} + \begin{bmatrix} 0 & -\omega_3 & \omega_2 \\ \omega_3 & 0 & -\omega_1 \\ -\omega_2 & \omega_1 & 0 \end{bmatrix} H = \begin{bmatrix} \tau_1 \\ \tau_2 \\ \tau_3 \end{bmatrix} + \text{disturbances} \quad [13d]$$

Equation [13d] is linearized with  $\delta\Omega = 0$  and quadratic terms in  $\omega$  dropped. Kinematic parameters are as usual introduced as small angles of frame  $B$  with respect to some desired inertial frame. Define these attitude parameters as  $\epsilon_n$ . The DPM is then:

$$\frac{dx}{dt} = Ax + B\tau \quad [14a]$$

$$A = \begin{bmatrix} 0 & \frac{-c_{32}h_w}{I_1} & \frac{+c_{22}h_w}{I_1} \\ \frac{+c_{32}h_w}{I_2} & 0 & \frac{-c_{12}h_w}{I_2} \\ \frac{-c_{22}h_w}{I_3} & \frac{+c_{12}h_w}{I_3} & 0 \end{bmatrix} \begin{matrix} 0_{3 \times 3} \\ \\ \end{matrix} \quad [14b]$$

$$B = \begin{bmatrix} \frac{1}{I_1} & & & & & \\ & \frac{1}{I_2} & & & & \\ & & \frac{1}{I_3} & & & \\ & & & 0_{3 \times 3} & & \end{bmatrix} \quad [14c]$$

$$\underline{x} = [\omega_1 \ \omega_2 \ \omega_3 \ \epsilon_1 \ \epsilon_2 \ \epsilon_3] \quad [14d]$$

It is found for HETE's mass properties that for control design assuming  $C_{PB} = I_{3 \times 3}$  is sufficient.

The following rules are applicable to the control strategies and plant described above and are useful to keep in mind. Their proofs follow from the dynamics and are straightforward but messy.

- Nutation damping is possible whenever a linear combination of  $\omega_1$  and  $\omega_3$  is observable and controllable. This is always possible unless  $\Psi$  approaches 0 or 180° and the controller remains in the partial authority mode.

- When a sun-sensor provides the only attitude measurement (as is the case for HETE during orbit day), rotation about the sensor boresight is unobservable. As shown in Figure 6, the axial coil's effect is to control, through gyroscopic coupling, rotation about  $\beta_p$ , the projection of field vector on the spin plane. Therefore, when in the partial authority actuator mode and  $\beta_p$  approaches the sun-sensor boresight, *controllability is reduced to that of using the wheel alone*. A pole/transmission zero cancellation at  $s = 0$  appears in the DPM under this condition.

- In the full authority actuator mode, steady-state disturbance rejection capability depends on the usual issues such as controller design, saturation, sensor noise. In the partial authority mode, an additional wrinkle is present. The disturbance torque can be broken into 3 components- an axial component, a spin-plane component orthogonal to  $\beta_p$ , and a spin-plane component parallel to  $\beta_p$ . According to [1], actuator authority exists to cancel the first two components only to the extent allowed by the performance of the controller. The effect of the third component is changed from that of a double integrator attenuated by an inertia to a single integrator attenuated by the stored angular momentum, which is a familiar result of rigid-body dynamics. *This is the fundamental benefit of a momentum-biased magnetic attitude control system*. Even when the field is unfavorable for using the full-authority actuator strategy, the effect of the uncontrollable disturbance component can still be significantly suppressed passively.

## V. Control Design for Partial Authority Mode

Since for the full-authority actuator mode the virtual control signals (torques which are converted to coil and wheel commands by inverting Eq. [2]) allow for a time-invariant controller design, the problem reduces to a standard one of stabilizing a momentum-biased body and will therefore not be discussed further here.

In the partial authority mode, the axial coil can generate control torques on the spin-plane along the direction  $\Theta \pm 90^\circ$ , and this inherent time-variation must be dealt with in the controller design. For cases where  $\Theta$  is expected to vary greatly while  $\Psi$  makes the full-authority mode inefficient, a single LTI controller robust to a wide range of  $\Theta$ 's would suffer greatly in performance. However, since the field direction changes slowly compared to the spacecraft's nutation dynamics, a time-varying controller where LQG gains are scheduled to the measured  $\Theta$  is found to perform quite well. The LQG form of the controller is chosen because it allows the implementation of a family of controllers with different eigenstructure simply by changing the gain elements. This ease of implementation is very desirable, and the restriction to a controller of the same order as the plant is found to not be a severe constraint for this problem. The robustness of this strategy to variations in nutation frequency, mass properties, and magnetometer measurement errors have been examined and found to be satisfactory. That analysis is omitted in this paper for brevity- see Ref. [10].

As noted, in the case of HETE the principal and body frames are close enough that for the sake of control design the assumption  $C_{PB} = I_{3 \times 3}$  is sufficient. This permits decoupling of the spin-axis wheel torque loop ( $1/s^2$  dynamics) and the spin-plane axial coil loop ( $1/s^2$  and nutation dynamics). For convenience, the two loops are lumped into one LQG design- the decoupling is implicit in the structure of the gain matrices obtained. Clearly, those gain elements relating to the wheel loop will be time-invariant (and in fact simply end up forming a lead compensator), while the other gain elements will vary as functions of  $\Theta$ .

The control design discussed below assumes full attitude measurement. As such, in HETE's case it applies only to the orbit night, when the UV instrument is providing attitude estimates. The implications of using only the sun-sensor during orbit day will be discussed afterwards.

Recall from Eq. [1] that the axial coil  $m_2$  generates a transverse torque  $\tau_t$  according to:

$$\tau_t = \begin{bmatrix} \beta_3 \\ 0 \\ \beta_1 \end{bmatrix} m_2 \quad [15]$$

It is desirable to eliminate the dependence on the field magnitude by defining a normalized control torque scalar  $\tau_{tN}$  such that:

$$\begin{aligned} \tau_t &= \begin{bmatrix} \frac{\beta_3}{\sqrt{\beta_1^2 + \beta_3^2}} \\ 0 \\ -\beta_1 \\ \frac{\beta_3}{\sqrt{\beta_1^2 + \beta_3^2}} \end{bmatrix} m_2 \sqrt{\beta_1^2 + \beta_3^2} \\ &= \begin{bmatrix} \cos(\Theta) \\ 0 \\ -\sin(\Theta) \end{bmatrix} \tau_{tn} \quad \tau_{tn} \equiv m_2 \sqrt{\beta_1^2 + \beta_3^2} \end{aligned} \quad [16]$$

The dependence on the transverse field component magnitude is thus eliminated, and the controller is designed to command  $\tau_{tn}$ . We therefore have a 2 dimensional control vector  $\underline{u}$  and an appropriate control distribution matrix which is a function of  $\Theta$  only:

$$B(\Theta) = B_0 B_{dir}$$

$$B_0 \equiv \begin{bmatrix} \frac{1}{I_1} & & \\ & \frac{1}{I_2} & \\ & & \frac{1}{I_3} \end{bmatrix}_{0_{3 \times 3}} \quad B_{dir} \equiv \begin{bmatrix} \cos(\Theta) & 0 \\ 0 & 1 \\ -\sin(\Theta) & 0 \end{bmatrix} \quad [17a]$$

$$\underline{u} = \begin{bmatrix} \tau_{tn} \\ \tau_w \end{bmatrix} \quad [17b]$$

As for the measurement, during orbit day the UV CCD camera and its data-reduction software provide the attitude measurement:

$$\underline{y} = [\epsilon_1 \quad \epsilon_2 \quad \epsilon_3]^T = C \underline{x} \quad C = [0_{3 \times 3} \mid I_{3 \times 3}] \quad [18]$$

In HETE's case, the UV instrument provides attitude solutions every 4 seconds, with roughly a 0.5 second delay which is found safe to ignore. The entire controller is thus implemented in discrete time with a sampling frequency of 0.25 Hz. The DPM is discretized using the standard zeroth-order hold equivalence:

$$\begin{aligned} \dot{\underline{x}}(t) &= A \underline{x}(t) + B(\Theta) \underline{u}(t) \quad \rightarrow \\ \underline{x}[n+1] &= \Phi \underline{x}[n] + \Gamma(\Theta) \underline{u}[n] \end{aligned} \quad [19]$$

The calculation of the discrete-time control distribution matrix is usually a series approximation to a convolution integral and would be cumbersome to compute on-line at each iteration of the LQG controller equations as the measured  $\Theta$

changes. This is not necessary, since it works out that:

$$\Gamma_0 = \left[ \int_0^T e^{A\eta} d\eta \right] B_0 \quad \Gamma(\Theta) = \Gamma_0 B_{dir} \quad [20]$$

where  $T$  is the sample time. Therefore,  $\Phi$  and  $\Gamma_0$  can be computed off-line, and  $\Gamma(\Theta)$  can be created easily given  $\Theta$ .

The control design methodology is made straightforward by available software such as MATLAB and is as follows:

- compute LQG filter gains (since the  $C$  matrix is constant, these gains do not vary WRT  $\Theta$ )
- cycle through  $360^\circ$  of  $\Theta$ , computing LQG regulator gains at each step
- approximate the regulator gain matrix as a function of  $\Theta$  with either sinusoidal or polynomial fit

The following was used for HETE's orbit night partial authority controller in this design study:

- dynamics:

$$\begin{aligned} [I_1 \quad I_2 \quad I_3] &= [4.86 \quad 5.41 \quad 4.08] \text{ Kg} \cdot \text{m}^2 \\ I_w &= 6.3 \times 10^{-3} \text{ Kg} \cdot \text{m}^2 \text{ (Ithaco Scanwheel)} \\ \Omega_0 &= 3000 \text{ RPM} \rightarrow h_w = 2 \text{ Nms} \end{aligned}$$

- noise intensities (define  $H$  = filter gain matrix):

$$\begin{aligned} E[\underline{w}[n] \underline{w}[n]^T] &= I_{3 \times 3} \quad E[\underline{v}[n] \underline{v}[n]^T] = 0.1 I_{3 \times 3} \\ \underline{w} &= \text{process noise, } \underline{v} = \text{measurement noise} \end{aligned}$$

- regulator cost function (define  $G$  = regulator gain matrix):

$$J = \frac{1}{2} \sum_{k=0}^{\infty} \left\{ \omega_1^2 + \omega_2^2 + \omega_3^2 + 10^{-2} (\epsilon_1^2 + \epsilon_2^2 + \epsilon_3^2) + \tau_{tn}^2 + \tau_w^2 \right\}$$

- compensator implementation:

- measure  $\Theta$ , compute  $B_{dir}$  and  $G(\Theta)$
- compensator state:  $\bar{\underline{x}}[n]$
- measurement vector:  $\underline{\epsilon}[n]$
- compensator input:  $e = -\underline{\epsilon}[n]$
- current estimate:  $\hat{\underline{x}}[n] = \bar{\underline{x}}[n] - H(e + C \bar{\underline{x}}[n])$
- control law:  $\underline{u}[n] = -G(\Theta) \hat{\underline{x}}[n]$
- prediction:  $\bar{\underline{x}}[n+1] = \Phi \hat{\underline{x}}[n] + \Gamma_0 B_{dir} \underline{u}[n]$

The computed filter gain matrix  $H$  is:

$$H = \begin{bmatrix} 0.5050 & 0 & 0.3319 \\ 0 & 0.5710 & 0 \\ -0.3569 & 0 & 0.5304 \\ 0.9315 & 0 & 0.0021 \\ 0 & 0.9403 & 0 \\ 0.0021 & 0 & 0.9425 \end{bmatrix}$$

The expected decoupling between the wheel loop and the axial coil loop is apparent in the zero elements. To see  $G(\Theta)$ , eq. [21] expands the control law output of the compensator.

$$\begin{aligned} \underline{u}[n] &= -G(\Theta)\underline{x}[n] \rightarrow \\ \tau_{in} &= g_{11}\omega_1 + g_{13}\omega_3 + g_{14}\epsilon_1 + g_{16}\epsilon_3 \\ \tau_w &= g_{22}\omega_2 + g_{25}\epsilon_2 \end{aligned} \quad [21]$$

Gain elements  $g_{22}$  and  $g_{25}$  corresponding to  $\tau_w$  are constant; the others associated with  $\tau_{in}$  are plotted in Figure 8. Their sinusoidal shapes make them easy to compute on-line as fitted functions of  $\Theta$ .

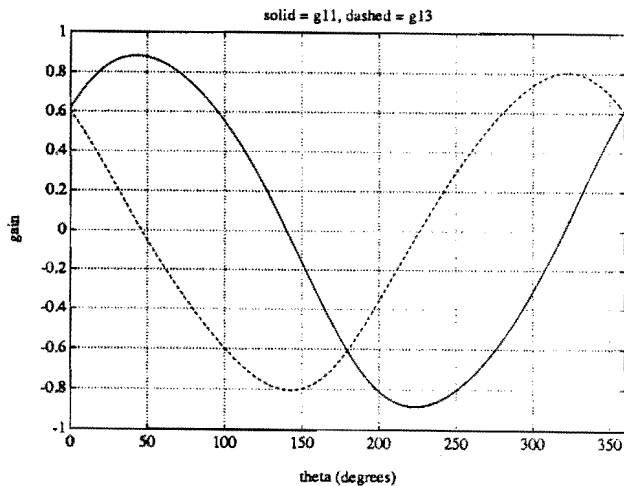


Figure 8a: LQR solutions for the  $\omega$  feedback gains  $g_{11}$  and  $g_{13}$  as functions of  $\Theta$

The separation principle applies to the closed loop poles:

$$\text{Filter Poles: } z = \text{eig}(\Phi - \Theta HC) \quad [22a]$$

$$\text{Regulator Poles: } z(\Theta) = \text{eig}(\Phi - \Gamma(\Theta)G(\Theta)) \quad [22b]$$

The filter poles are invariant WRT  $\Theta$ ; they end up at  $s =$ :

$$\begin{aligned} &-0.4137 + 0.2879i \\ &-0.4137 - 0.2879i \\ &-0.2785 + 0.7415i \\ &-0.2785 - 0.7415i \\ &-0.3523 + 0.4350i \\ &-0.3523 - 0.4350i \end{aligned}$$

when mapped to the  $s$ -plane via the relation  $s = \text{Log}(z)/T$ . The achieved closed loop regulator poles are also mapped to the  $s$ -plane and are plotted in Figure 9 as  $\Theta$  is varied:

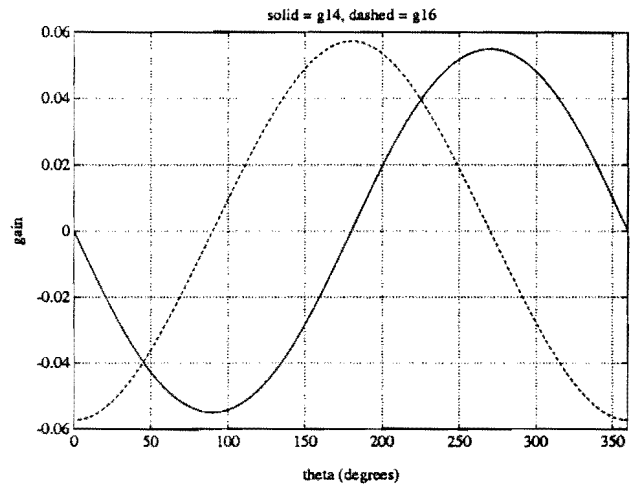


Figure 8b: LQR solutions for the  $\epsilon$  feedback gains  $g_{14}$  and  $g_{16}$  as functions of  $\Theta$

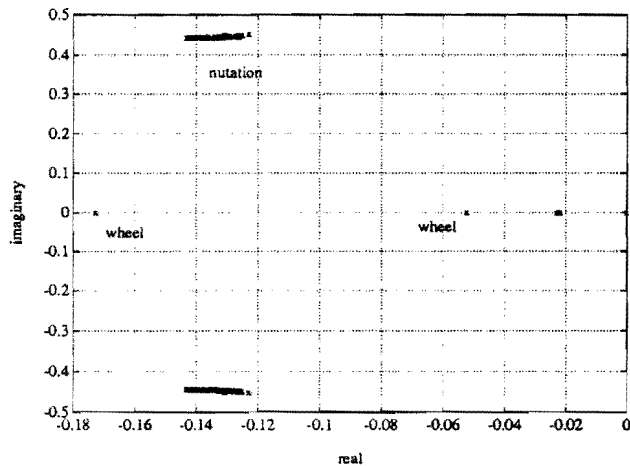


Figure 9: closed loop regulator root locus, mapped to the  $s$ -plane via  $z = e^{sT}$ . The parameter  $\Theta$  is varied over a  $2\pi$  range.

It is seen that the gain-scheduled controller achieves consistent stabilization of the plant over the full range of  $\Theta$ , provided  $\Theta$  varies slowly compared to the dynamics. Examining the eigenstructure of the closed loop system, recall the open loop poles of the DPM: 4 integrators and 2 nutation poles on the  $j\omega$  axis. On Figure 9, the poles labeled "wheel" have eigenvectors with non-zero elements along  $\omega_2$  and  $\epsilon_2$  only. They represent two of the four open loop integrators and are moved by the wheel control loop, showing the expected decoupled behavior. The complex pair labeled

"nutation" have complex conjugate eigenvectors with components along  $\omega_1$ ,  $\omega_3$ ,  $e_1$ , and  $e_3$ . They are the damped open loop nutation poles and exhibit some variation WRT  $\Theta$ . Of the remaining two open loop integrators, one is moved to  $s = -0.02$ . The remaining integrator is not moved and has an eigenvector with zero  $\omega$  components and  $e$  components pointed orthogonal to  $\beta_p$ . This uncontrollable mode which occurs when using the partial authority actuator has a clear geometric interpretation which has been alluded to. Since the axial coil generates torques orthogonal to  $\beta_p$ , gyroscopic coupling removes controllability of rotation about this axis. It is significant that the uncontrollable mode's eigenvector contains no  $\omega$  components. This is because gyroscopic stiffness prevents any transverse rates from having 1/s dynamics, as discussed earlier. Note that transmission zeros are not plotted in Figure 9, but that one certainly exists at  $s = 0$ .

The control design shown above is for the partial authority actuator mode during orbit night. The major differences for orbit day, when the sun-sensor replaces the UV instrument as the attitude sensor, are:

- Rather than switching to full-authority mode when the field is "bad," the axial coil loop is turned off until the field improves. The wheel loop is left operational, of course.
- The field is "bad" when  $\Psi$  approaches 0 or 180° (the penalty factors as shown in Figure 5), or when  $\Theta$  approaches the sun-sensor boresight, as discussed in Section IV. Taking into account errors in the  $\Theta$  measurement (which depend on the magnetometer and on  $|\beta|$ ), the axial coil loop cutoff threshold is set at  $\Theta = \pm 20^\circ$  from the sun-sensor boresight.
- The attitude measurement is degraded and analog, so less aggressive control gains and a pre-filter are used. The orbit day control loop runs with a sampling frequency of 1Hz.

## VI. Simulation Results

Simulation study of the designed controllers were carried out. Some design issues not addressed above were incorporated in simulation runs:

- Minimization of controller transients upon switching actuator modes is important, especially transients in rate response since they affect pointing stability. It is found that rate transients on controller start-up are excited mostly by initial

attitude errors. Reduction of the controller bandwidth to counter this effect is unsatisfactory, as it would result in reduced disturbance rejection. The strategy which proved useful is essentially the same as "profiling" servo commands. Upon switching actuator modes (and therefore controllers as well), the current attitude is defined as the "null" reference frame. Attitude errors fed to the controller are then measured with respect to the new null frame, and profiled attitude commands are issued relative to the null frame to bring the spacecraft to the desired celestial referenced attitude. Therefore, initial attitude errors are by definition zero, and switching transients are minimized. Attitude command profiles continuous to the second derivative were found to be satisfactory.

- A simple anti-windup scheme of software-saturating the commanded torquer moments and using this as the input to the estimator portion of the LQG controller proved sufficient in simulation.

Modeling issues addressed in the simulation include the use of an 8th order Earth field model (IGRF 1985 coefficients, see Ref. [8] and [9]), disturbance torque models, and hardware imperfection models. For the latter:

- mass properties:
  - 10° separation between frame **B** and **P**
  - 15% nutation freq. offset from design point
- 3-axis magnetometer:
  - 120/1024  $\mu\text{T}$  resolution
  - 3  $\mu\text{T}$  bias
  - 5° misalignment per axis
- sun sensor: 10/1024 deg. resolution
- mag. torquers:
  - 8/256  $\text{Am}^2$  resolution
  - 10% coil factor offset
  - 4  $\text{Am}^2$  max moment
  - 5° misalignment per axis
- momentum wheel:
  - $8 \times 10^{-4}$   $\text{rad/s}^2$  acceleration resolution (corresponds to 5  $\mu\text{Nm}$  torque resolution)
  - 5%  $I_w$  offset
  - 20  $\text{mNm}$  torque saturation (never reached)
  - 5° axial misalignment

Two potentially important effects- reaction wheel rumble and details of the attitude solutions from the UV instrument- were omitted at the time

of this study. Disturbance torque modeling included:

- solar pressure (DC due to sun-point attitude)
- $0.2 \text{ Am}^2$  spacecraft residual dipole (following recommendations of Ref. [11])
- atmospheric disturbance using  $\rho = 2 \times 10^{-13} \text{ Kg/m}^3$ ,  $v = 7.6 \text{ Km/s}$ , and an elementary shadowing model
- gravity gradient

A representative spectrum of the disturbance model output is shown in Figure 10.

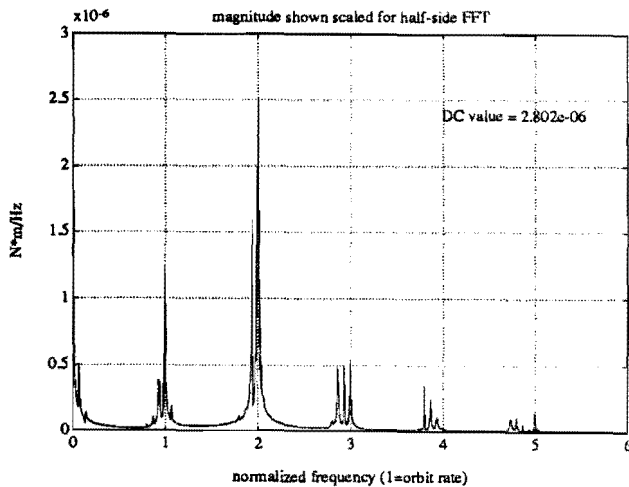


Figure 10: a representative spectrum of the output from the external disturbance model used in simulation

**Simulation Case 1:** the scenario is that the transition from orbit night to day occurs at  $t = 0$ , and the larger rates from orbit day must be damped before the start of science observations.

- orbit night controller
- switch from full to partial authority actuator occurs at around  $t = 550 \text{ s}$
- initial rates:  $\omega = [30 \ 30 \ -30] \text{ }^\circ/\text{hr}$ ;

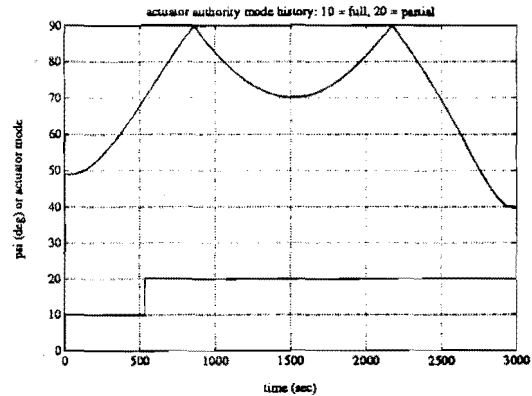


Figure 11a:  $\Psi$  and actuator mode history for this simulation case. Note the  $90^\circ$  to  $180^\circ$  half of  $\Psi$  have been wrapped to the 1st quadrant to make implementation of the Schmidt trigger easier.

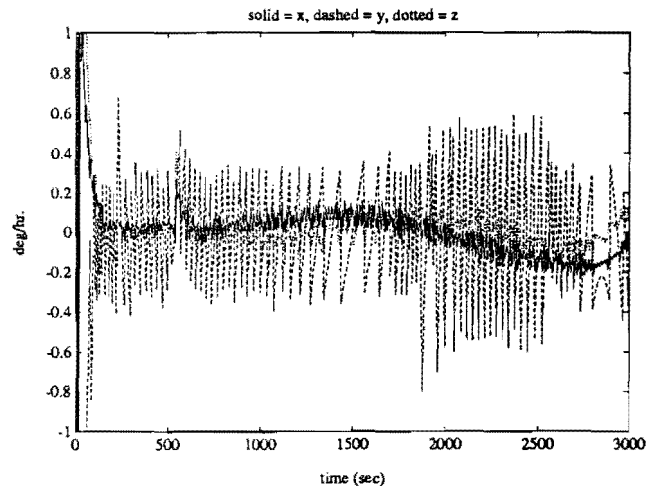
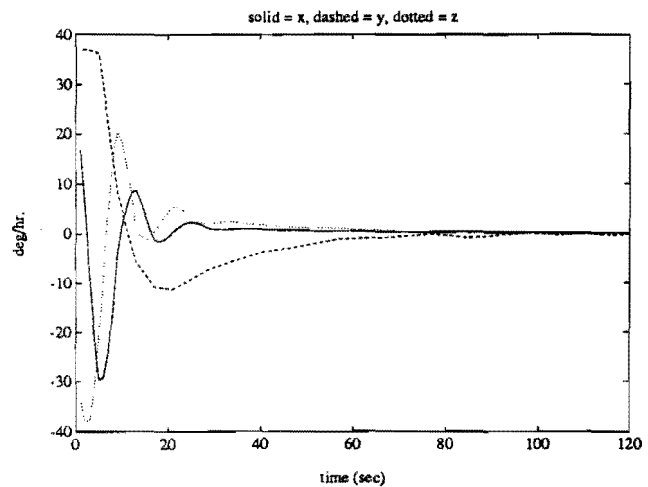


Figure 11b: rate history, closeup near  $t = 0$  (top) and full plot (bottom). Recovery from initial rate is nice, and transients incurred during actuator mode switch is minimal. Larger  $y$  rate limit cycle is due to wheel control torque quantization.

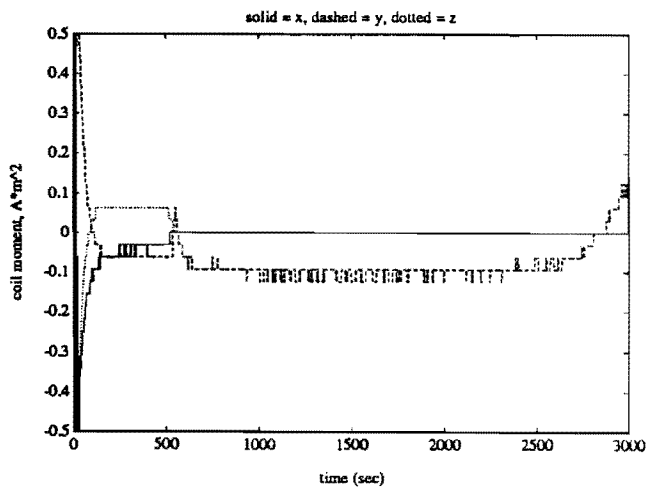
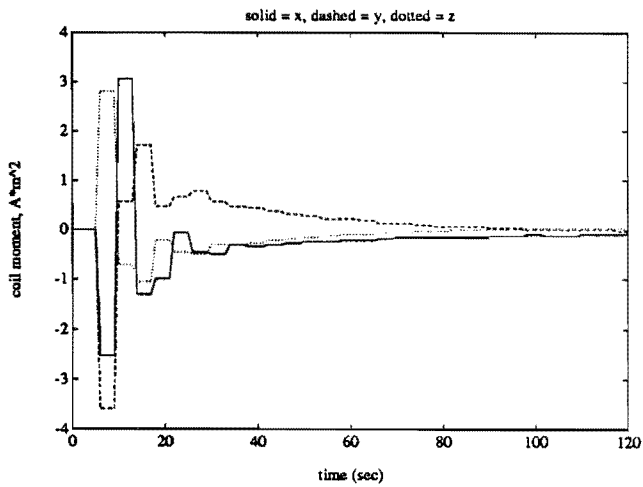


Figure 11c: torquer activity history, closeup near  $t=0$  (top) and full plot (bottom). Note that  $m_1 = m_3 = 0$  in partial authority actuator mode.

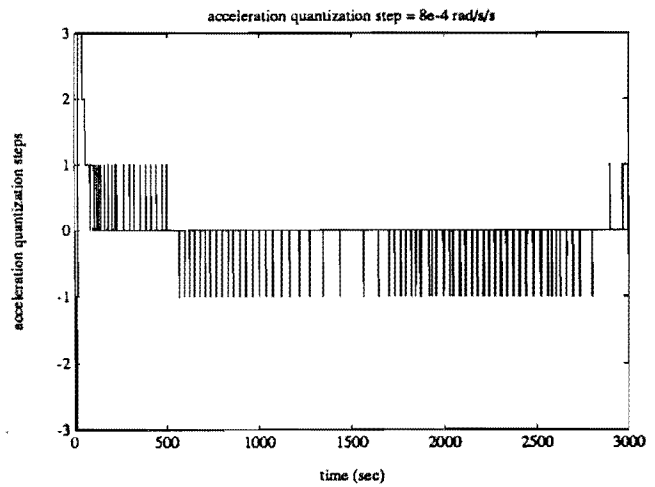
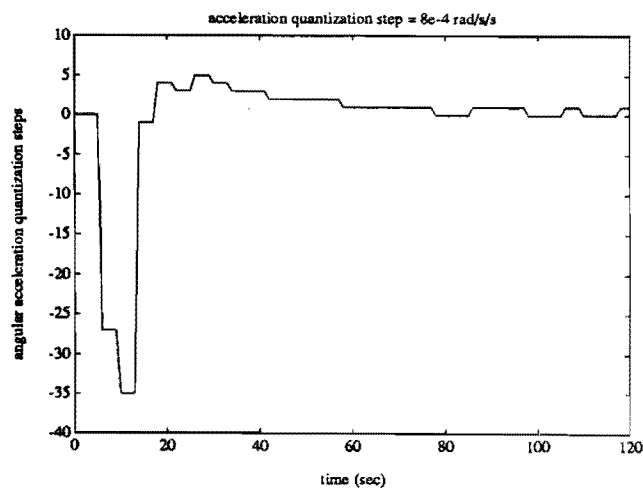


Figure 11d: wheel acceleration history, closeup near  $t = 0$  (left bottom) and full plot (above).

Simulation Case 2: same scenario as in case 1, except the field history encountered is such that the controller starts in the partial authority actuator mode and transitions to the full authority mode at  $t \approx 2000$  sec. As expected, the initial rate damping performance is worse but still acceptable. The disturbance rejection performance improvement in the full authority mode is evident in Figure 12b.

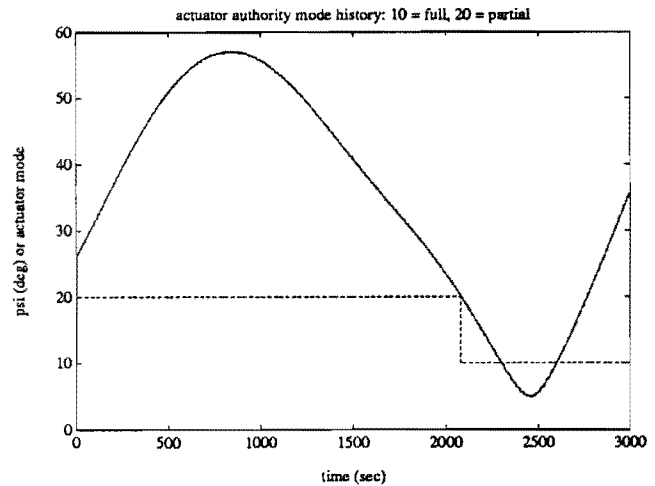


Figure 12a:  $\Psi$  and actuator mode history, same convention as in Fig. 11a.

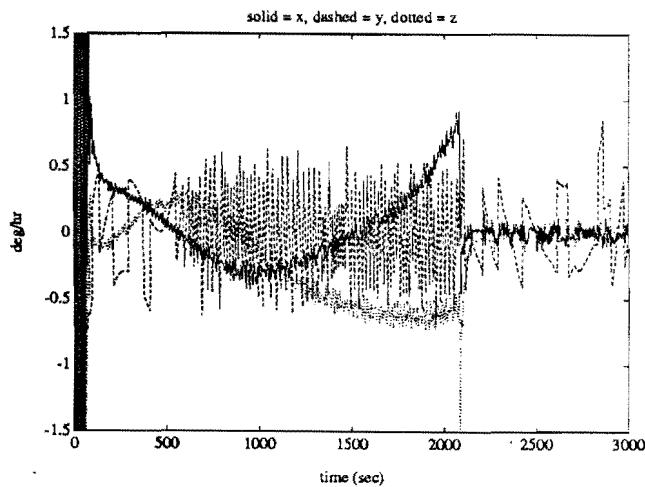
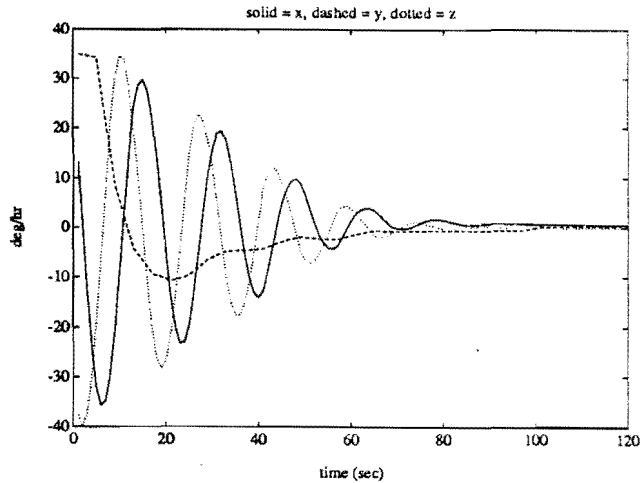


Figure 12b: rate history; note the lighter damping of initial nutation and improved performance upon switching to full authority. Note also transient incurred from mode switch is successfully minimized.

**Simulation Case 3:** performance of the orbit-controller is demonstrated in this example. The simulation scenario shows:

- recovery from a large initial rate error of  $[-100 \ -120 \ -100]$  °/hr and a sun point initial error of  $5^\circ$  azimuth and  $3^\circ$  elevation
- momentum management, assuming initial  $\delta\Omega = 50$  RPM, which is much worse than the expected accumulation after one orbit night
- forced idle of the axial-coil control loop when  $\Theta$  gets within  $20^\circ$  of 0 (sun-sensor boresight)

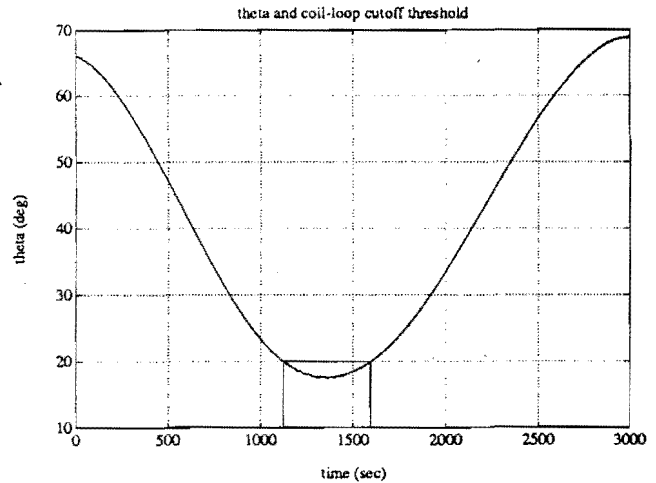


Figure 13a:  $\Theta$  history for this simulation; the box represents when the axial-coil control loop is idled, as discussed in Section V.

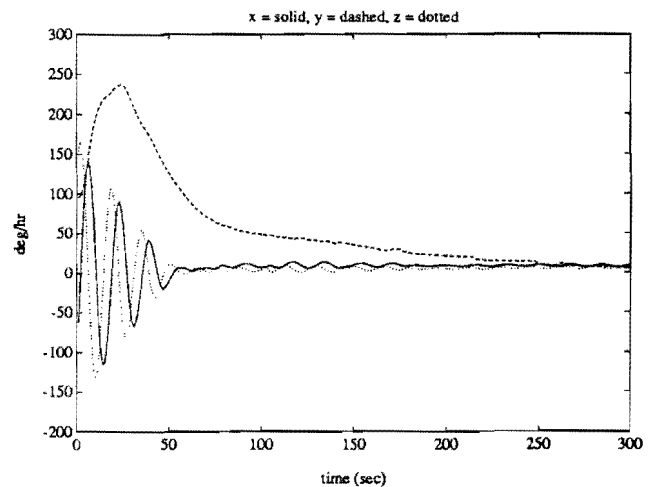


Figure 13b: closeup near  $t=0$  showing acceptable rate recovery performance; large transient in  $y$  rate is due to wheel loop reducing azimuth error.

## VII. Conclusions

Actuator strategies and accompanying control designs have been presented to take maximum advantage of arbitrary field vector directions in magnetic and momentum bias controlled satellites. Performance suitable for nadir or inertially stabilized spacecrafts with moderately tight pointing and rate requirements are shown to be achievable in simulations for the HETE small satellite. The resulting algorithms are simple to implement and well within current on-board processing capabilities.

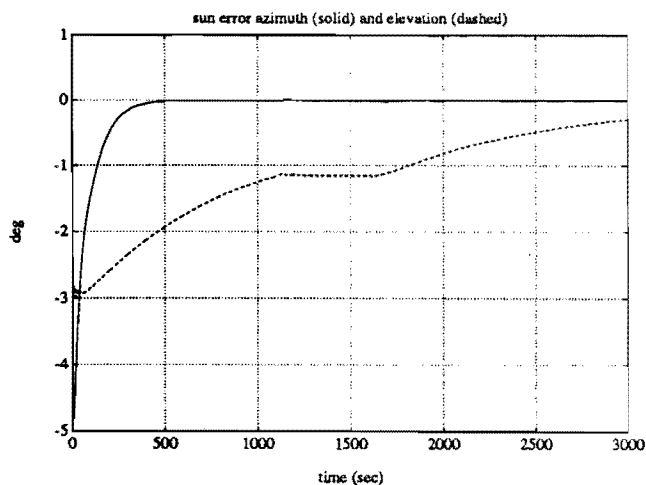


Figure 13c: sun point error; note coil loop is considerably less effective than wheel loop at sun tracking, as expected; note also the period of coil loop shut down during bad  $\Theta$

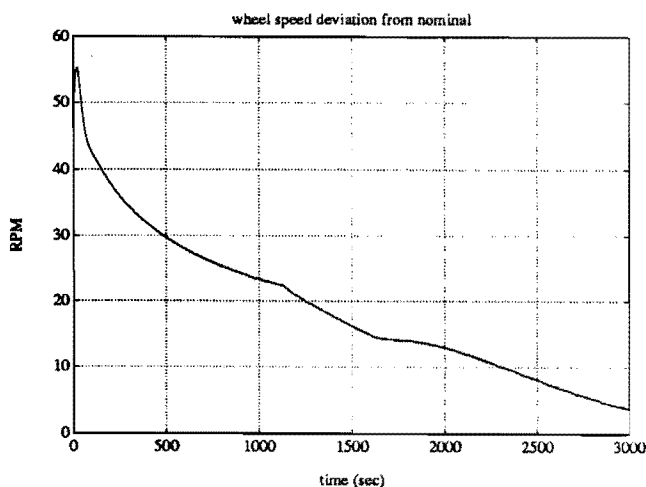


Figure 13d:  $\delta\Omega$  history showing effect of momentum management loop

### Acknowledgments

The author is grateful for the help of staff at the MIT Center for Space Research and at Aero-Astro Inc. of Herndon, VA., especially John Doty and Richard Warner. Most of the preliminary HETE spacecraft system design is credited to Aero-Astro Inc.

### References

[1] Collins, D.H. and Bonello, D.P., "An Attitude Control System for Earth Observation Spacecraft." AIAA paper 73-854.

[2] Stickler, A. C. and Alfriend, K. T., "An Elementary Magnetic Attitude Control System." AIAA paper 74-923.

[3] Mobley F.F., Konigsberg, R., and Fountain, G. H., "Attitude Control of the SAS-C Satellite." AIAA paper 74-901

[4] Ricker, G. et. al., *Proposal to NASA for a High Energy Transient Experiment*. Submitted by the Center for Space Research, MIT, Cambridge, MA. 1987.

[5] Tascione, Thomas F: *Introduction to the space environment*. Orbit Book Co., Malabar, FL, 1988.

[6] Wertz, James R. (editor): *Spacecraft Attitude Determination and Control*. D. Reidel Publishing Co., Holland/Boston, 1978.

[7] NASA: *Magnetic Fields, Earth and Extraterrestrial*. NASA SP-8017, March 1969.

[8] Barraclough, D. R. and Kerridge, D. J.: *IGRF 1985 Grid Point Values and Charts*. IAGA Bulletin #52, International Union of Geodesy and Geophysics, Paris 1986.

[9] Malin, S.R.C. and Barraclough, D.R.: "An Algorithm for Synthesizing the Geomagnetic Field." *Computers and Geosciences*, Vol. 7, No. 4, pp. 401-405, 1981.

[10] Chang, D. H.: "Attitude Control System for the High Energy Transient Experiment Small Satellite." M.S. Thesis, MIT Dept. of Aeronautics and Astronautics, Cambridge, MA. May 1991.

[11] NASA: *Spacecraft Magnetic Torques*. NASA SP-8018, March 1969.